Journal of Crystal Growth 310 (2008) 3968–3972

Contents lists available at ScienceDirect

Journal of Crystal Growth

journal homepage: www.elsevier.com/locate/jcrysgro

Semi-insulating GaN substrates for high-frequency device fabrication

J.A. Freitas Jr.[a,*], M. Gowda[a,b], J.G. Tischler[a], J.-H. Kim[c], L. Liu[d], D. Hanser[d]

[a] Naval Research Laboratory, Washington, DC 20375, USA
[b] Department of ECE, George Mason University, VA 22030, USA
[c] Department of Chemical and Biological Engineering, Korea University, Seoul 136-701, South Korea
[d] Kyma Technologies Inc., Raleigh, NC, USA

ARTICLE INFO

Available online 18 June 2008

PACS:
78.30.Fs
81.05.Ea
78.40.Fy
78.55.m
71.70.Ch
71.35.–y

Keywords:
A1. Characterization
A1. Impurities
A1. X-ray diffraction
A3. Hydride vapor phase epitaxy
B1. Nitrides
B2. Semiconducting materials

ABSTRACT

Thick *c*-plane unintentional doped and iron-doped GaN substrates were grown by hydride vapor phase epitaxial technique on sapphire substrates. The morphology and crystalline quality of the freestanding samples show no evident degradation due to iron doping. Low-temperature photoluminescence measurements show reduction of the exciton-bound to neutral impurities band intensities with iron doping increase. Near-infrared photoluminescence studies confirm the incorporation and activation of iron impurities. Variable temperature resistivity measurements verified that the iron-doped films are semi-insulating.

1. Introduction

Unintentionally doped (UID) GaN films grown on foreign substrates such as sapphire or SiC are characterized by high concentration of threading and screw dislocations, typically between 10^9 and $10^{10}\,cm^{-2}$ and background free carriers concentration in the range between 10^{17} and 10^{18} electrons/cm^3 [1,2]. These templates have been successfully used for the fabrication and commercialization of a number of optoelectronic and high-frequency devices [3–5]. Presently, the development of devices requiring lower leakage current and current threshold, higher breakdown voltage, and higher room-temperature carrier mobility are on hold for materials with lower concentration of extended defects and larger grain boundary [6–9]. It is expected that such requirement would be achievable if GaN films are deposited on native GaN substrates.

Due to the relatively high growth rate, hydride vapor phase epitaxial (HVPE) technique has been establishing as a promising approach to accomplish the growth of large area and/or bulk GaN native substrates. Freestanding (FS) HVPE GaN substrates are accomplished by separation of thick GaN films grown on sacrificial substrates such as sapphire and GaAs [10–12]. Thick crack-free films with diameter up to 3 in. have been reported [13]. These substrates are becoming commercially available for epitaxial layer deposition and device fabrication. UID GaN heteroepitaxial films and FS HVPE substrates have an undesirable background donor impurities, mostly Si and/or O, which results in a room-temperature free carrier net concentration typically between low 10^{17} to high 10^{18} electrons/cm^3 [14]. Intrinsic n-type conductivity may be adequate for light-emitting devices such as LED and LD, but it is unacceptable for high-power/high-frequency devices fabrication, which require semi-insulating (SI) substrates to block current leakage.

To mitigate the relatively high-intrinsic concentration of free carriers, a number of growers have used impurities such as Be, C, Fe, and Zn to compensate the pervasive shallow donors in GaN and to achieve the desirable SI substrate characteristics [15–17]. Among these impurities, Fe seems to be the most adequate impurity because the $Fe^{3+/2+}$ acceptor level is only about 0.34 eV below the bottom of the conduction band [18]. It is expected that this deep acceptor level will efficiently compensate the GaN free carriers at typical devices operating temperatures. In fact, it has been demonstrated that iron-doped HVPE GaN substrates can reproducibly achieve resistivity of about $3\times10^5\,\Omega$/cm at 250 °C [19]. Despite this accomplishment, there are no detailed studies

* Corresponding author. Tel.: +1 202 404 4536; fax: +1 202 767 1165.
E-mail addresses: jaime.freitas@nrl.navy.mil (J.A. Freitas Jr.), hyunhyun@korea.ac.kr (J.-H. Kim).

0022-0248/$ - see front matter © 2008 Elsevier B.V. All rights reserved.
doi:10.1016/j.jcrysgro.2008.06.038

investigating the dilution limits and doping efficiency of iron in GaN, and only recently the effects of GaN morphology and iron-doping uniformity have been reported [20].

This work reports the optical and electronic properties of FS HVPE GaN substrates, both nominally undoped and iron doped, grown on sacrificial sapphire substrates. We observed no evidence of deterioration of material optical and structural properties on iron doping.

2. Experimental procedure

The GaN samples were grown on a vertical HVPE hot-wall reactor, at sub-atmospheric pressure. The GaCl precursor was produced by reaction between HCl and liquid Ga in the upstream part of the reactor, which is kept at 915 °C. Bis(cyclopentadienyl) iron (Cp_2Fe) was used as the iron source for the Fe-doped GaN crystals, which was introduced into the reactor via a N_2 carrier gas. The GaN films were deposited on *c*-plane (0 0 0 1) sapphire substrates with an AlN nucleation layer, in the downstream part of the reactor where the GaCl and the NH_3, transported by N_2 gas, reacts. GaN growth was carried out at substrates temperatures of approximately 1000 °C. The growth rate of the films was 150 μm/h. Thick layers (1–2 mm) were grown and removed from the underlying sapphire to create FS, bulk material. The layers were characterized in the as-grown state, i.e., without polishing or surface preparation. Polar and non-polar GaN layers grown using this process have been previously shown to possess very good structural properties [21,22]. The doping level of similarly grown Fe-doped crystals in the same system was measured via secondary ion mass spectrometry (SIMS) to be around $1 \times 10^{18}\,cm^{-3}$.

The crystalline properties of the undoped and iron-doped samples were probed by X-ray diffraction (XRD) measurements using a Philips X'pert MRD triple axis diffracted beam system. The morphologies of these samples were verified by SEM and SEM panchromatic cathodoluminescence-imaging (SEM/CLi) techniques, and by real color (RGB) photoluminescence imaging (PLi) using a HeCd laser to excite the samples, at room-temperature. Low-temperature photoluminescence (PL) spectroscopy was employed to verify the optical and electronic properties of the samples. The PL system comprised an 1800 groves/mm double gratings spectrometer and an UV-extended GaAs photomultiplier couple to a computer control photon-counter. The samples were placed in a continuous flow He cryostat, which allows temperature variations between 1.5 and 330 K. The luminescence was excited with the 325 nm line of a HeCd laser, which power density was controlled with calibrated neutral density filters.

The incorporation of the iron impurity, and the activation of $Fe^{3+/2+}$ compensating acceptors were corroborated by low-temperature near-infrared (NIR) PL spectroscopy. The samples were placed at a cold-finger cryostat and excited with the 808 nm line of a diode laser. The light emitted by the samples was dispersed by a Princeton/Acton Trivista 557 triple spectrometer fit with an LN_2 cool OMA V InGaAs linear array detector.

3. Results and discussion

The full width at half maximum (FWHM) of the (0 0 0 2) XRD peak measured at the FS substrate AE492.7 is only 90 arcsec as shown in Fig. 1a and the FWHM of the (1 0 $\underline{1}$ 2) XRD peak is 146 arcsec (not shown), which is consistent with a high-crystalline quality material and is representative of the X-ray linewidth of other measured samples. Real-color PL imaging of the UID GaN substrate AE498.11, represented in Fig. 2a, has an intense red color

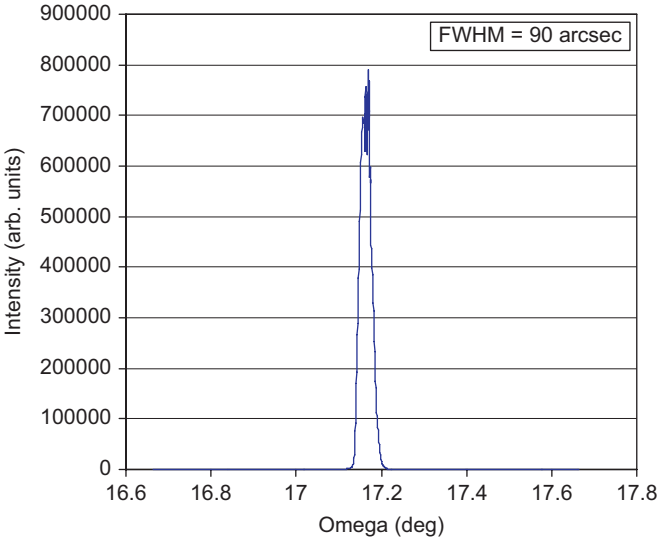

Fig. 1. XRD spectrum of one of the Fe-doped thick freestanding GaN substrate.

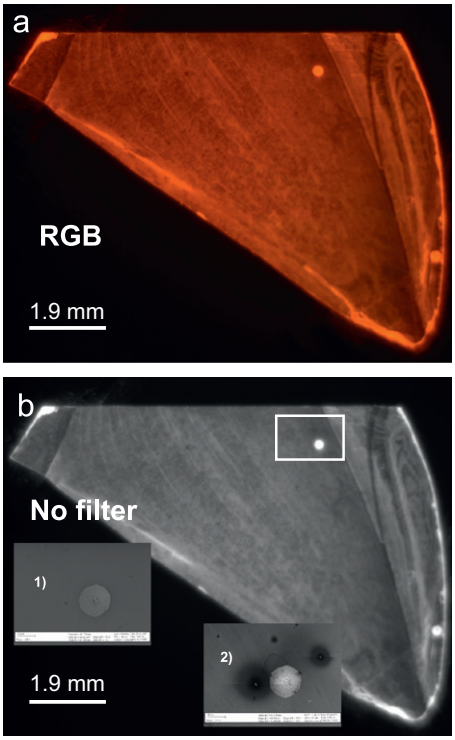

Fig. 2. (a) RGB PL imaging of UID GaN film grown on AlN/sapphire template. (b) Panchromatic PL imaging of the sample shown in (a). The insets (1) and (2) show the SEM/CL and SEM/imaging of the region highlighted in (a), respectively.

hue emission. Fundamental colors imaging show that red is the dominant emission, with an intense green and weak blue contribution. The color and intensity distribution is quite uniform, and only two hexagonal base pyramid defects are observed at the sample surface. The PL panchromatic imaging of this sample, represented in Fig. 2b, also shows a quite uniform distribution of intensity, with few dark spots. The panchromatic SEM/CLi of the white boundary rectangular region indicated in the sample imaging, inset (1), confirms the good sample uniformity. SEM imaging of the same highlighted region depicted on inset (2), due to high-current contrast, shows clearly the presence of pits, which

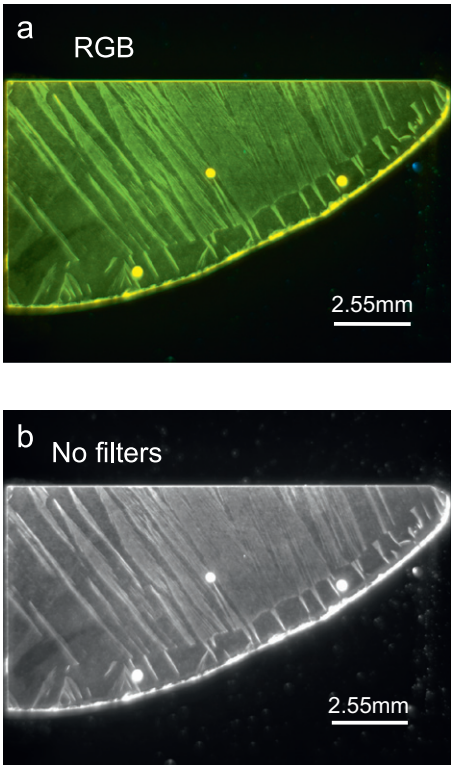

Fig. 3. (a) RGB PL imaging of a Fe-doped GaN substrate. (b) Panchromatic PL imaging of the sample represented in (a). *Note*: the bright "palm tree leaves" shape defects.

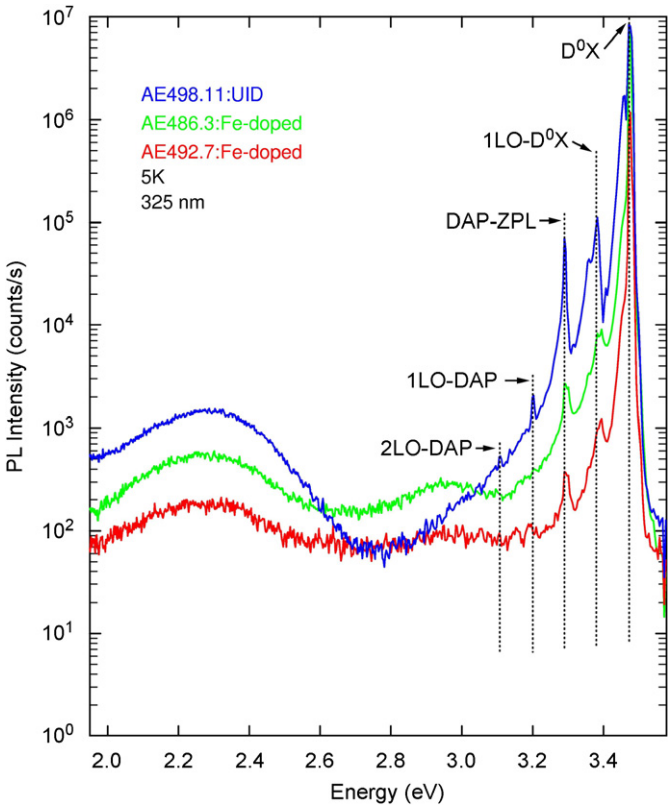

Fig. 4. Low-resolution and low-temperature PL spectra of undoped and iron-doped samples. *Note*: the reduction of all luminescence bands with the iron doping.

are weakly observed in the SEM/CLi picture. Similar experiments were performed on the iron-doped samples. Fig. 3a shows the RGB PL imaging of the iron-doped sample AE492.7. This imaging shows a green-yellow color hue, which results from the mixture of a relatively weak green contribution with less intense red and an extremely weak blue emissions components. It is clearly seen in Fig. 3a non-uniform distribution of luminescence intensity across the sample. Bright regions with "palm tree leaves" shape appear across the samples. Such features, not yet identified, are not related to the iron doping, because they have been observed in UID substrates. Panchromatic imaging of this sample, depicted in Fig. 3b, reveals the same features observed in the RGB PL image. SEM and SEM/CL images of this sample clearly demonstrate that the morphology of this sample is similar to that of the UID sample.

To probe changes in the electronic properties of HVPE GaN substrates with iron doping, we performed a detail low-temperature PL measurement in one UID (AE498.11) and two iron-doped (AE486.3 and AE492.7) samples, which are represented in Fig. 4, in the spectral range between 1.97 and 3.57 eV. The spectrum of the UID substrate (AE498.1), top spectrum in Fig. 4, shows the typically intense and dominant emission line near 3.47 eV (D^0X), which is associated with the recombination process involving the annihilation of excitons bound to neutral shallow donors, leaving the donors in the ground state. (The nomenclature used in the present manuscript was previously introduced by Freitas et al. in Ref. [23]). Also observed are the less intense first phonon replica of D^0X near 3.38 eV (1LO-D^0X), the zero-phonon line of the shallow-donor/shallow-acceptor pair (DAP) recombination near 3.29 eV and their phonon replicas (nLO-DAP) at lower energies, a weak broad luminescence band around 3.0 eV, and the so-called yellow band at 2.25 eV. We also observe a relatively intense red band, which peaks around 1.75 eV. Due to the difficulties to provide a short and clear explanation about the nature of deep centers in GaN, the latter features will not be discussed. Note that all bands

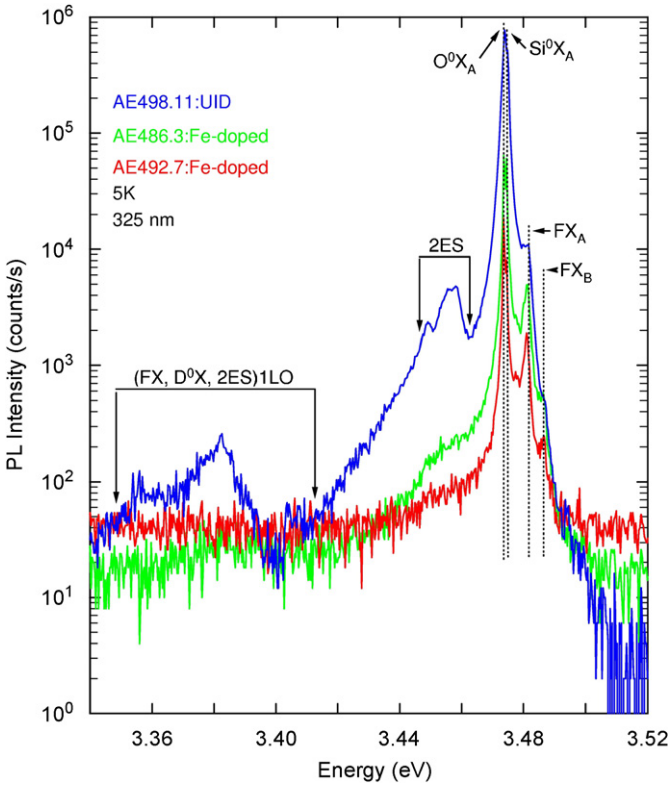

Fig. 5. High-resolution and low-temperature PL spectra of the samples represented in Fig. 4, in the band-edge spectral region.

observed in the spectrum of the UID sample are reproduced in the spectra of the iron-doped samples. However, it is important to point out that the relative intensity of all these bands decreases with increasing of the iron doping. This observation is consistent with the change in the room-temperature PL-imaging intensity. Fig. 5 depicts the PL spectra of all samples represented in Fig. 4, in the spectral region between 3.34 and 3.52 eV. The spectrum of UID sample show emission lines related to the ground state of the free-exciton B (FX_B), the ground state of the free-exciton A (FX_A), and the dominant exciton bound to neutral Si and O donors ($S_i^0X_A$ and O^0X_A). Around 3.45 eV, we detect the so-called two-electron satellite (2ES) spectrum resulting from the recombination processes that leave neutral donors in an excited state after the exciton annihilation. Spectral separations between D^0X and 2ES lines yield the intra-center transition energies of the impurities. Note that for energies below 3.42 eV, we observe the one-phonon replicas of all features listed above, represented as (FX, D^0X_A, 2ES) 1LO. All the features observed in the spectrum of the UID samples are replicated in the spectrum of the iron-doped samples. Again, note that their relative intensities reduce with iron doping. In addition, the relativity intensity of the FX_A and FX_B lines to the intensity of the D^0X line increase. This is consistent with the compensation of the neutral shallow Si and O donors by the iron impurities, which moves the Fermi level from the bottom of the conduction band towards the center of prohibit gap.

Low-temperature NIR-PL measurements were carried out in all samples to verify the incorporation and activation of iron impurities. Fig. 6 depicts the NIR-PL spectra of the two iron-doped samples, AE486.3 and AE492.7. The intense line at 1.299 eV, represented in Fig. 6, is associated with the $^4T_1(G) \rightarrow {}^6A_1(S)$ crystal-field transition of the iron substitutional for the Ga atom, i.e., Fe^{3+}_{Ga} [18,24]. The relatively broad additional lines observed in both samples spectra are the phonon sideband structure. We observed a small spectral intensity variation between the two Fe-doped samples, which may be associated with different concentration of Fe^{3+}_{Ga}. PL measurements performed on different regions of these samples showed no sizable variations of the peak intensity and energy position, indicating no local stress and concentration variation, i.e., PL intensity for the samples were spatially very homogeneous.

The resistivity of the Fe-doped GaN samples was measured via temperature dependent Hall effect. Ti (250 Å)/Al(1250 Å) contacts with an Au capping layer were used on the sample. The contacts were annealed at 600 °C prior to measurement. Fig. 7 shows the resistivity calculated from the Hall-effect measurements as a function of 1000/T for a Fe-doped GaN sample. The room-temperature resistivity was greater than $10^{10}\,\Omega$/cm [25]. The activation energy of the deep level in the GaN was determined to be 1.14 eV. This result indicates that high-quality SI GaN substrates for high-frequency device fabrication can be produced.

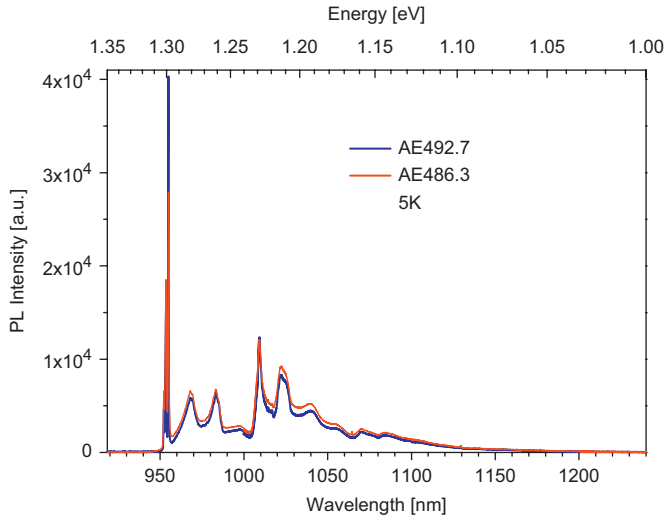

Fig. 6. Low-temperature NIR-PL spectra of the two Fe-doped samples. The intense emission line at 1.299 eV is related to substitutional Fe impurities.

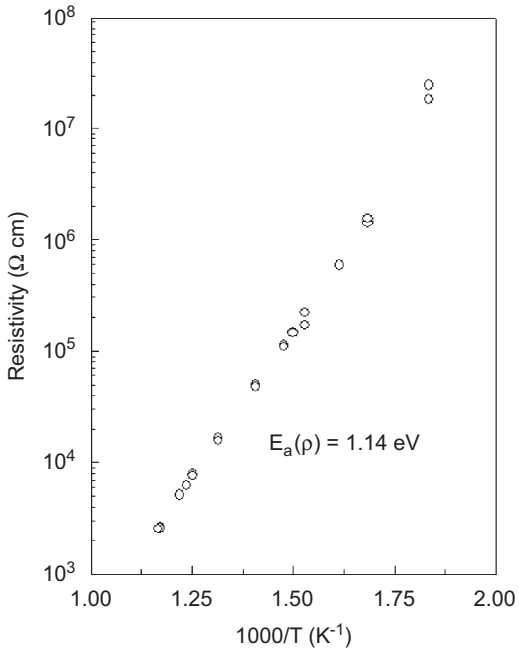

Fig. 7. Fe-doped GaN resistivity as a function of 1000/T as determined by Hall-effect measurements.

4. Summary

High-crystalline quality UID and iron-doped FS GaN films grown by HVPE process on sapphire with AlN nucleation layer can be reproducibly grown. No deterioration of the morphology and the structural and optical properties of the substrates were observed on Fe-doped substrates. Low-temperature PL studies of these samples are consistent with full compensation of the pervasive Si and O shallow donors. In addition, the low-temperature NIR PL shows that the incorporation of Ga substitutional Fe^{3+} compensating centers was realized. Temperature-dependent Hall measurements clearly indicate the SI GaN substrate was achieved.

Acknowledgments

Dr. J.-H. Kim was supported by ONR-Global (N00014-06-1-4046) and by Brain Korea 21 program.

References

[1] H.M. Ng, D. Doppalapudi, T.D. Moustakas, N.G. Weimann, L.F. Eastman, Appl. Phys. Lett. 73 (1998) 821.
[2] M. Sakai, H. Ishikawa, T. Egawa, T. Jimbo, M. Umeno, T. Shibata, K. Asai, S. Sumiya, Y. Kuraoka, M. Tanaka, O. Oda, J. Crystal Growth 244 (2002) 6.
[3] I. Akasaki, J. Crystal Growth 300 (2007) 2.
[4] S.M. Hubbard, G. Zao, D. Pavlidis, W. Sutton, E. Cho, J. Crystal Growth 284 (2005) 297.
[5] Y. Cordier, M. Azize, N. Baron, S. Chenot, O. Tottereau, J. Massies, J. Crystal Growth 309 (2007) 1.

[6] C.D. Lee, A. Sagar, R.M. Feenstra, W.L. Sarney, L. Salamanca-Riba, J.W.P. Hsu, Phys. Status Solidi A 188 (2001) 595.
[7] D. Jenna, A.C. Gossard, U.K. Mishra, Appl. Phys. Lett. 76 (2000) 1707.
[8] D. Jenna, U.K. Mishra, Appl. Phys. Lett. 80 (2002) 64.
[9] P. Kozodoy, J.P. Ibbetson, H. Marchand, P.T. Fini, S. Keller, J.S. Speck, S.P. DenBaars, U.K. Mishra, Appl. Phys. Lett. 73 (1998) 975.
[10] M.K. Kelly, R.P. Vaudo, V.M. Phanse, O. Ambarcher, M. Stutzmann, Jpn. J. Appl. Phys. 38 (1999) L217.
[11] S.S. Park, I.-W. Park, S.H. Choh, Jpn. J. Appl. Phys. Part 2 39 (2000) L1141.
[12] K. Motoki, T. Okahisa, N. Matsumoto, M. Matsushima, H. Kimura, H. Kasai, K. Takemoto, K. Uematsu, T. Masahiro, M. Nakayama, S. Nakahata, M. Ueno, D. Hara, Y. Kumagai, A. Koukitu, H. Seki, Jpn. J. Appl. Phys. Part 2 40 (2001) L140.
[13] T. Yoshida, Y. Oshima, T. Eri, K. Ikeda, S. Yamamoto, K. Watanabe, M. Shibata, T. Mishima, J. Crystal Growth 310 (2008) 5.
[14] W.J. Moore, J.A. Freitas Jr., G.C.B. Braga, et al., Appl. Phys. Lett. 79 (2001) 2570.
[15] D.F. Storm, D.S. Katzer, J.A. Mittereder, S.C. Binari, B.V. Shanabrook, X. Xu, D.S. McVey, R.P. Vaudo, G.R. Brandes, J. Crystal Growth 281 (2005) 32.
[16] A. Armstrong, C. Poblenz, D.S. Green, U.K. Mishra, J.S. Speck, S.A. Ringel, Appl. Phys. Lett. 88 (2006) 082114.
[17] R.P. Vaudo, X. Xu, A. Salant, J. Malcarne, G.R. Brandes, Phys. Status Solidi (a) 200 (2003) 18.
[18] R. Heitz, P. Maxim, L. Eckey, P. Thurian, A. Hoffmann, I. Broser, K. Pressal, B.K. Meyer, Phys. Rev. B 55 (1997) 4382.
[19] N.I. Kuznetsov, A.E. Nikolaev, A.S. Zubrilov, Y.V. Melnik, V.A. Dmitriev, Appl. Phys. Lett. 75 (1999) 3138.
[20] J.A. Freitas Jr., J.G. Tischler, J.-H. Kim, Y. Kumagai, A. Koukitu, J. Crystal Growth 305 (2007) 403.
[21] D. Hanser, L. Liu, E.A. Preble, D. Thomas, M. Williams, Mater. Res. Soc. Symp. Proc. 798 (2004) Y2.1.1.
[22] T. Paskova, R. Kroeger, S. Figge, D. Hommel, V. Darakchieva, B. Monemar, E. Preble, A. Hanser, N.M. Williams, M. Tutor, Appl. Phys. Lett. 89 (2006) 051914.
[23] J.A. Freitas Jr., W.J. Moore, B.V. Shanabrook, G.C.B. Braga, S.K. Lee, S.S. Park, J.Y. Han, Phys. Rev. B 66 (2002) 233311.
[24] J. Baur, K. Maier, M. Kunzer, U. Kaufmann, J. Schneider, H. Amano, I. Akasaki, T. Detchprom, K. Hiramatsu, Appl. Phys. Lett. 64 (1994) 857.
[25] Y. Kumagai, K. Takemoto, H. Murakami, A. Koukitu, Jpn. J. Appl. Phys. 44 (2005) L1072.